High-pressure x-ray diffraction experiments on icosahedral Ti-Zr-Ni - unusual effects due to a low shear modulus and a high Poisson's ratio

2000 J. Phys.: Condens. Matter 12 8071

(http://iopscience.iop.org/0953-8984/12/37/306)

J. Phys.: Condens. Matter **12** (2000) 8071–8080. Printed in the UK PII: S0953-8984(00)14359-0

High-pressure x-ray diffraction experiments on icosahedral Ti–Zr–Ni—unusual effects due to a low shear modulus and a high Poisson's ratio

U Ponkratz, R Nicula, A Jianu and E Burkel

Universität Rostock, Fachbereich Physik, August-Bebel-Strasse 55, D-18051 Rostock, Germany

Received 31 May 2000, in final form 9 August 2000

Abstract. *In situ* high-pressure x-ray diffraction experiments have been performed on quasicrystalline Ti–Zr–Ni in energy-dispersive mode using synchrotron radiation. Pressures up to 30 GPa were generated using a diamond anvil cell. The bulk modulus of Ti–Zr–Ni was determined to be $B_0 = 166$ GPa $\pm$ 13 GPa. Some of the experiments were performed under slightly non-hydrostatic conditions. In these runs, deviations from a standard equation of state could be observed and these are due to additional strains. According to the model of Singh and Kennedy for elastically isotropic solids, these strains are proportional to the non-hydrostatic stress component and indirectly proportional to the shear modulus of the sample. From our measurements, the shear modulus of icosahedral Ti–Zr–Ni was estimated to be $\mu \approx 7$ GPa with a relative error of about 50%. This value is low compared to the shear moduli of icosahedral Al–Cu–Fe, Al–Pd–Mn (for both, $\mu \approx 65$ GPa) and Al–Li–Cu ($\mu = 38$ GPa). The Poisson's ratio of Ti–Zr–Ni was determined to be $\nu = 0.48 \pm 0.015$. This value is close to the maximum value which is allowed by the laws of thermodynamics, namely $\nu = 0.5$. The Poisson's ratios of common metals ($\nu \approx 1/3$) and other icosahedral alloys like Al–Cu–Fe ($\nu = 0.19$), Al–Pd–Mn ($\nu = 0.28$) and Al–Li–Cu ($\nu = 0.25$) are much lower.

1. Introduction

Since the discovery of quasicrystals in 1984 [1], studies have been mainly devoted to the formation, structure and stability against temperature, while studies concerning the high-pressure properties of these materials are still rare. The first high-pressure investigations were performed on icosahedral Al–Mn alloys which were found to be stable up to pressures of 28 GPa [2] and 47 GPa [3], respectively. On the other hand, Al–Li–Cu undergoes an irreversible amorphization at pressures of about 20 GPa [4]. In the last few years, interest was focused on the high-pressure properties of the thermally stable Al–Cu–TM (TM: transition metal) and Al–Pd–TM phases. It was found that Al–Cu–Fe [5, 6], Al–Cu–Re [7], Al–Pd–Mn [8] and Al–Pd–Ru [7] are stable up to pressures of about 35 GPa. Recently, the stability of Al–Pd–Mn [9] and decagonal Al–Ni–Co [10] up to 70 GPa were demonstrated. All these high-pressure studies were conducted on Al-based quasicrystalline alloys. In recent years, Ti-based alloys were discovered which also form stable icosahedral phases. These materials are interesting from a technical point of view due to their ability to store hydrogen [11, 12]. The stability of the icosahedral structure under pressure is important for sintering processes and various high-pressure synthesis procedures. The first high-pressure study on Ti–Zr–Ni has shown that this material is stable up to pressures of 30 GPa [13, 14]. Strong deviations from an equation of state could be observed and are reported in the present paper. These effects include

0953-8984/00/378071+10$30.00

quasilattice constant increase under pressure as well as hysteresis loops being produced during pressure cycles. Similar effects have been reported for the compression curves of Cu_3Au [15], a ductile, elastically anisotropic material. In this case, the high-pressure behaviour can be explained in terms of plastic deformation caused by non-hydrostatic stresses and local microstresses at the grain boundaries due to elastic anisotropy. However, these explanations cannot be used for Ti–Zr–Ni since icosahedral alloys are known to be brittle and elastically isotropic.

2. Experimental procedure

The $Ti_{52.8}Zr_{26.2}Ni_{21}$ samples were prepared by single-roller melt spinning in a protective Ar atmosphere. The resulting alloys formed ribbons 1 cm to 10 cm long having an average cross-section of 2 mm × 50 μm. Small sample grains were obtained by dry grinding in an agate mortar. The *in situ* high-pressure x-ray diffraction experiments were performed using synchrotron radiation at the F3 beamline of HASYLAB/DESY synchrotron radiation laboratory (Hamburg, Germany) in energy-dispersive mode. More information on the experimental station can be found in [16]. The diffraction angle was chosen to be about 5° and was calibrated using a gold foil. The relation between the interplanar distance d, x-ray energy E and diffraction angle Θ is given by

$$d\ (\text{Å}) = \frac{6.199}{\sin\Theta\ E\ (\text{keV})}. \tag{1}$$

For the primary and scattered beams, tungsten collimation slits were used. Scattered photons were collected in an energy range from 14 keV to 68 keV using a Ge solid-state detector. Pressures were generated using a gas-membrane diamond anvil cell (DIACELL) equipped with 500 μm diameter diamonds. The samples were enclosed in a 150 μm diameter hole in a 200 μm thick Inconel gasket preindented to about 50 μm. A single flake of Ti–Zr–Ni was loaded together with sodium chloride as the pressure-transmitting medium and internal pressure marker. Pressures were calculated using the (200) diffraction line from sodium chloride. This was done using a Birch equation of state with parameters $B_0 = 24.03$ GPa and $B_0' = 4.71$ obtained from a fit to the data of Decker [17]. During one run, a ruby chip was added for cross-checking the pressure calibration using the ruby fluorescence method. In this case, pressures were calculated using the formula given in reference [18]. All experiments have been performed at room temperature.

The indexing of the icosahedral reflections was done using the method proposed by Cahn *et al* [19]:

$$q = \frac{1}{d_{N,M}} = \frac{1}{a_6}\frac{\sqrt{N + M\tau}}{\sqrt{2(2+\tau)}}. \tag{2}$$

Here q is the scattering vector in parallel space, $\tau = (1+\sqrt{5})/2$ is the golden mean and a_6 is the hypercubic lattice parameter in the six-dimensional hyperspace. The diffraction patterns were analysed by profile matching with Lorentz and Pearson VII functions. The hypercubic lattice parameter was calculated using the icosahedral reflections (18, 29), (20, 32) and (52, 84). To check whether the compression was isotropic, the pressure dependence of the d-spacing ratios $d(18, 29)/d(20, 32)$, $d(18, 29)/d(52, 84)$ was calculated. These ratios are constant for all pressures within an error of 0.3%

The pressure dependence of the hypercubic lattice parameter is described using the Birch equation of state

$$p = \frac{3}{2}B_0\left[\left(\frac{a}{a_0}\right)^{-7} - \left(\frac{a}{a_0}\right)^{-5}\right]\left[1 + \frac{3}{4}(B_0' - 4)\left[\left(\frac{a}{a_0}\right)^{-2} - 1\right]\right] \tag{3}$$

where B_0 is the zero-pressure bulk modulus and B_0' the first pressure derivative.

It must be noted that the volume of the unit cells cannot be determined directly with x-ray diffraction; only the values of the lattice spacings are accessible. Furthermore, in the energy-dispersive geometry used in the present experiments, only lattice spacings which lie nearly perpendicularly to the incident beam contribute to the diffracted intensity (see also figure 4). This will be discussed in more detail in section 4.

3. Results

The evolution of the relative hypercubic lattice parameter of Ti–Zr–Ni under increasing pressure is shown in figure 1. Different symbols correspond to three different sample loadings. Although every sample behaves differently in the pressure range between 0 GPa and 8 GPa, the behaviour of all samples can be grouped into three stages: an initial stage of high compressibility is followed by a stage of hardening. Finally we observe a stage of lattice parameter increase.

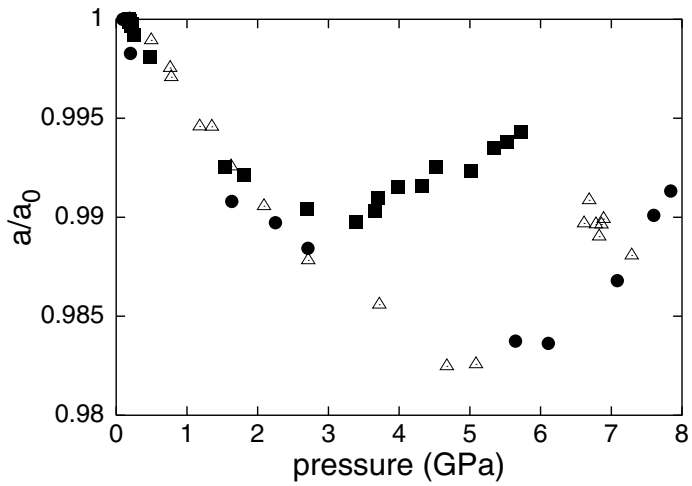

Figure 1. The dependence of the relative hypercubic lattice constant a/a_0 of Ti–Zr–Ni on the pressure. The symbols correspond to three different runs.

During the initial stage of compression, from 0 GPa to 2–3 GPa, the samples show a very high compressibility. In this stage of compression the bulk modulus has values in the range $B_0 \approx 60$–90 GPa. These values are lower than the bulk moduli of pure Ti ($B_0 = 106$ GPa), Zr ($B_0 = 94.4$ GPa) and Ni ($B_0 = 179$ GPa) [20]. From 2–3 GPa to 4–6 GPa, the Ti–Zr–Ni samples seem to harden, i.e. the compressibility decreases. In the pressure range from 4–6 GPa to approximately 8 GPa, the quasilattice seems to increase. This is evidenced by the fact that the NaCl diffraction lines shift towards higher energies (indicating decreasing lattice parameters), whereas the diffraction lines of the icosahedral phase shift to lower energies (indicating increasing lattice parameters), as shown in figure 2.

For data points collected at pressures above 8 GPa, the quasilattice parameter decreases with increasing pressure. However, fitting a Birch EOS to data points collected above 8 GPa is only possible if one assumes a zero-pressure hypercubic lattice constant of $a/a_0 \approx 1.0071$. This behaviour is reflected by all three icosahedral reflections observed, which correspond to fivefold symmetry, (18, 29), and twofold symmetry, (20, 32) and (52, 84). In different runs, all samples were found to behave in the same way. However, the value of the initial

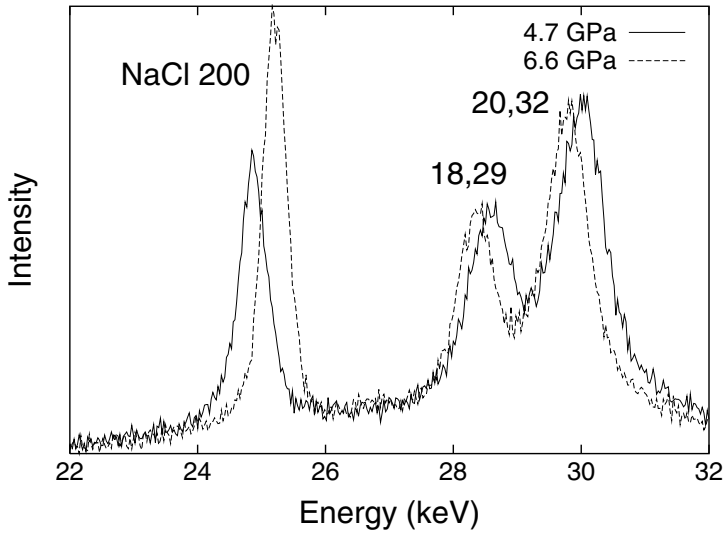

Figure 2. Diffraction patterns of Ti–Zr–Ni at 4.7 GPa and 6.6 GPa. The (200) reflection of NaCl is shifted towards higher energies; the reflections (18, 29) and (20, 32) are shifted to lower energies.

compressibility and also the onset pressure of the quasilattice parameter increase were different for different runs.

Another set of experiments were performed in cycles, i.e. spectra were collected during compression, pressure release and second pressure increase. During the first compression the behaviour was identical to the one just described: phases of low compressibility, hardening and lattice parameter increase could be observed. On pressure release, the resulting decompression curve does not lie on the initial pressure-increase curve but on a curve which is an extrapolation to lower pressures of the data points collected above 8 GPa during pressure increase. In the pressure range between 2 GPa and 4 GPa, the quasilattice parameters are larger than the one at ambient pressure ($a_6 = 7.16$ Å).

However, after pressure release to 0 GPa, the same hypercubic lattice parameter as before the experiment was found. Thus, large hysteresis loops in the p–V diagrams were observed (figure 3). When the pressure is increased for a second time, the data points lie on to the previous pressure-release curve. The lattice spacings start to increase upon pressure increase, reach their maximum values at about 2 GPa and decrease monotonically for all pressures above that (empty squares in figure 3). These hysteresis loops have been observed for several runs. None of these effects are due to effects of bridging by the sample grains between the diamond anvils. This hypothesis was ruled out on the basis of our observations of the sample volume by optical microscopy.

4. Discussion

The behaviour presented in the previous section can be explained by taking into account the presence of a uniaxial stress component inside the diamond anvil cell. To describe the stress conditions, we employ a rectangular coordinate system with stress components σ_1 and σ_2 parallel and σ_3 perpendicular to the diamond faces. The stress component σ_3 is parallel to the direction of the external force acting on the diamond anvils. Since the sample volume of a diamond anvil cell has a cylindrical symmetry, it is assumed that $\sigma_1 = \sigma_2$. The uniaxial

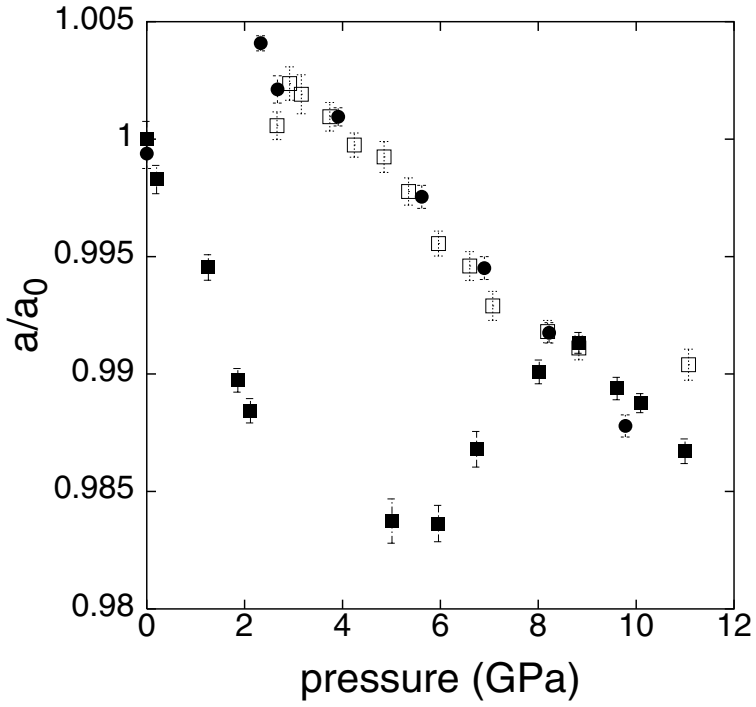

Figure 3. The hysteresis loop of Ti–Zr–Ni during first compression (filled squares), pressure release (filled circles) and second compression (empty squares). Pressure was calibrated using the ruby fluorescence method.

stress component is defined as $t = \sigma_3 - \sigma_1$. The hydrostatic pressure σ_p is given by $\sigma_p = (\sigma_1 + \sigma_2 + \sigma_3)/3 = (\sigma_1 + t/3)$. It is common for compressive stresses and strains resulting from them to be taken to be negative.

The behaviour of cubic crystals under non-hydrostatic conditions has been investigated in great detail by A K Singh and G C Kennedy [21, 22]. The authors demonstrated that the strain in diffraction experiments depends on the crystallographic direction and on the elastic anisotropy coefficient of the sample. Inelastic neutron scattering experiments and ultrasonic measurements on icosahedral alloys showed that phonon dispersion modes and sound velocities are independent of quasicrystallographic directions [23]. From this point of view it is justified to treat icosahedral alloys as elastically isotropic solids. For elastically isotropic solid the Singh–Kennedy equation simplifies to

$$\epsilon = \epsilon^p + \epsilon^t = \frac{\sigma_p}{3B} - \frac{t}{3}(1 - 3\cos^2\Psi)\frac{1}{2\mu} \tag{4}$$

where ϵ^p describes the lattice strain under hydrostatic conditions and ϵ^t is the strain caused by non-hydrostatic stress, B is the bulk modulus, t the value of the uniaxial stress component, μ the shear modulus of the sample and Ψ is the angle between the stress direction and the normals of the diffracting lattice planes (figure 4).

According to equation (4), in the presence of a uniaxial stress component the value of the lattice parameter depends on the direction in which it is measured. A non-hydrostatic stress component will cause an additional strain which is proportional to t and indirectly proportional to the shear modulus μ. Since typical diffraction angles Θ are in the range of 3° to 7° and t is expected to be collinear with the incoming beam, the angle Ψ is close to 90°. With t

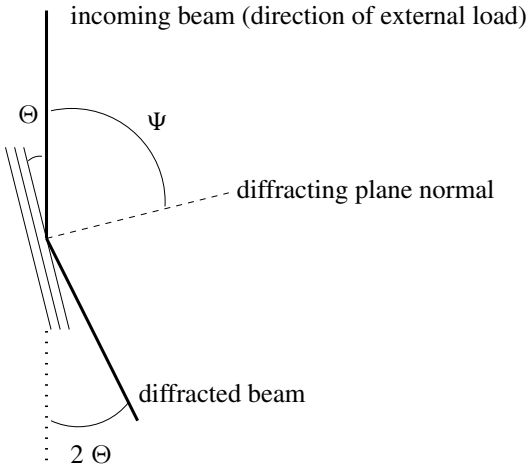

Figure 4. The diffraction geometry in the energy-dispersive x-ray diffraction experiments using a diamond anvil cell. Note that only lattice planes with normals nearly perpendicular to the incoming beam contribute to the diffracted intensity.

being defined to be negative, the resulting strain ϵ^t will be positive. This corresponds to an additional expansion of the quasilattice (see also figure 2 of [24]). One should note that a positive (compressive) additional strain will be measured if one observes lattice planes with normals parallel to the external load ($\Psi = 0^\circ$).

It has been found that the stress component t tends to saturate at certain values (maximum shear stress or the von Mises criterion) [22]:

$$|t| \leqslant \sigma_y \approx 2\ \tau_y \tag{5}$$

where σ_y is the yield strength and τ_y is the shear strength of the sample material or of the pressure-transmitting medium. In the experiment described here, the maximum value t_s is related to the shear strength of sodium chloride. This is supported by the fact that the Ti–Zr–Ni flakes maintained the same shapes up to the highest pressures applied. The yield point of the sample material was not reached: this would have resulted in a deformation or fracture of the sample grain. The shear modulus and Poisson's ratio of icosahedral Ti–Zr–Ni could not previously be determined directly, since strain gauge measurements, inelastic neutron scattering experiments and sound velocity measurements require single-domain samples measuring at least some cubic millimetres. The shear modulus of the sample can be calculated with equation (4) if the uniaxial stress component is known exactly. To determine the uniaxial stress component caused by sodium chloride, it is necessary to determine the positions of the Bragg reflections of NaCl corresponding to different symmetry directions. From these, t can be calculated using the theory of Singh and Kennedy for elastically anisotropic solids. However, in the experiments described here, the counting times were too short, so just the position of the (200) reflection of sodium chloride could be determined with the accuracy required. High-pressure experiments on Cu_3Au foils embedded in NaCl in a diamond anvil cell [15] showed that the uniaxial stress component in NaCl has a value $t \approx -0.3$ GPa for hydrostatic pressures below 14 GPa. These data scatter strongly between -0.2 GPa and -0.4 GPa. Also, the reported errors for each value are about 0.1 GPa. To estimate the shear modulus, we assume that the uniaxial stress component has a saturation value of -0.3 GPa. It should be noted also that the maximum stress value t_s depends on pressure. Experiments on pure NaCl in an opposed-anvil device [25] showed that t rises to -0.5 GPa at hydrostatic pressures of

about 20 GPa. Since the aim of the present paper is just an estimation of the shear modulus of Ti–Zr–Ni, this effect will be neglected here.

With increasing hydrostatic pressure, also non-hydrostatic stresses inside the pressure-transmitting medium start to develop. The expansive strain resulting from non-hydrostatic stress is larger than the strain due to hydrostatic compression. Thus, a lattice increase with pressure can be noticed. After the uniaxial stress component reaches its saturation value t_s, a constant additional strain ϵ^t will be observed, i.e. the resulting p–V curve is shifted with respect to the compression curve in the hydrostatic case (figure 5). This difference is

$$\delta\epsilon = \epsilon^t = -\frac{t_s}{3}(1 - 3\cos^2\Psi)\frac{1}{2\mu}. \tag{6}$$

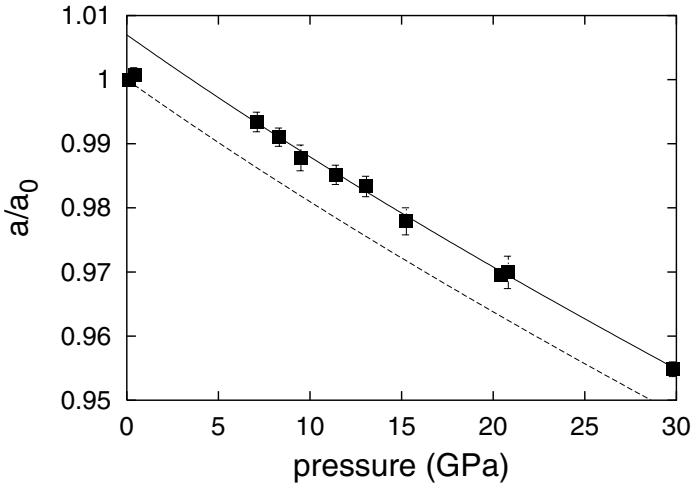

Figure 5. The dependence of the relative hypercubic lattice constant on the pressure. The solid line is a fit with a Birch EOS ($B_0 = 166$ GPa, $B_0' = 1.9$ and $a_0 = 1.0071$); the dashed line corresponds to a calculated Birch EOS with the same values for B_0 and B_0'. The difference between the two curves is the strain component ϵ^t due to non-hydrostatic compression.

As mentioned above, a Birch EOS can only be fitted to the data if one assumes a relative hypercubic lattice constant of 1.0071 at zero pressure. Making the approximation $\cos^2\Psi \approx 0$, one gets

$$\epsilon^t = \frac{-t_s}{6\mu} \approx 0.0071. \tag{7}$$

Using $t_s = -0.3$ GPa, one finds, for the shear modulus of Ti–Zr–Ni, $\mu \approx 7$ GPa with a relative error of about 50 %. This error is due to the fact that the value of t is not known exactly. The estimated shear modulus of Ti–Zr–Ni is low compared to the shear moduli of icosahedral Al–Cu–Fe, Al–Pd–Mn (both $\mu \approx 65$ GPa) [6,8] and Al–Li–Cu ($\mu \approx 38$ GPa) [26]. Using the bulk modulus of Ti–Zr–Ni ($B_0 = 166$ GPa), one can calculate the Poisson's ratio ν:

$$\nu = \frac{B_0 - \frac{2}{3}\mu}{2B_0 + \frac{2}{3}\mu}. \tag{8}$$

For Ti–Zr–Ni, we find $\nu = 0.48 \pm 0.015$. This value is close to the maximum value of $\nu = 0.5$ allowed by the laws of thermodynamics. The Poisson's ratios of common metals ($\nu \approx 0.3$) [27] and other icosahedral alloys like Al–Cu–Fe ($\nu = 0.19$) [6], Al–Pd–Mn ($\nu = 0.28$) [8] and Al–Li–Cu ($\nu = 0.25$) [26] are much lower.

The behaviour during the initial compression, i.e. a low bulk modulus and a lattice size increase in the pressure region between 5 GPa and 8 GPa, still needs to be explained. A material with a high Poisson's ratio has a Young's modulus Y which is lower than the bulk modulus:

$$Y = 3B_0(1 - 2\nu). \tag{9}$$

A low Young's modulus corresponds to a high compressibility in the direction of the applied load. This fact explains the low bulk modulus determined during the initial pressure increase. As can be seen in figure 4, the lattice planes contributing to the scattered intensity are aligned nearly perpendicularly to the incoming beam (and the external force). Since a stage of high compressibility is observed at the beginning, the uniaxial stress component cannot be collinear with the external force. The reason for this is that the sample grain is inhomogeneously surrounded by NaCl grains of different sizes and shapes. Thus the external load is transmitted via a large number of NaCl grains, so the resulting stress at the sample position may have a different direction with respect to the external load. At higher hydrostatic pressures of about 5 GPa to 8 GPa, the NaCl grains get compacted until the sample grain is embedded in a more homogeneous environment. This effect was observed with optical microscopy: during the initial stage the view of the sample grain is rather blurred; for pressures above 8 GPa the pressure medium becomes homogeneous and optically more transparent.

During the process of compacting of the sodium chloride grains, the uniaxial stress component changes its direction; after the compacting process is completed, the uniaxial stress component has the same direction as the external load. Thus, the angle Ψ in equation (4) changes to $\Psi = 90^\circ - \Theta \approx 90^\circ$, so the sign of ϵ^t reverses which results in an increase of the quasilattice parameter.

In the following, a simple model is introduced which describes the behaviour of icosahedral Ti–Zr–Ni. Since at the beginning of the experiment the angle Ψ is not 90°, it was arbitrarily assumed that $1 - 3\cos^2\Psi = -1$. Furthermore, it was assumed that the uniaxial stress component increases linearly with pressure. The observed data can be described very well with $t(p) = 0.12\,\sigma_p$. Thus t reaches its maximum value of -0.3 GPa at a pressure of 2.5 GPa (region **1** in figure 6). After t has reached a saturation value of -0.3 GPa, the non-hydrostatic stress component remains constant. This corresponds to a constant additional compressive strain of $\epsilon \approx -0.0078$. The situation is unchanged until a hydrostatic pressure of $\sigma_p = 5$ GPa is reached (region **2** in figure 6). Between 5 GPa and 8 GPa the pressure medium gets compacted. The uniaxial stress component will change its direction until it is collinear with the direction of the external load. In our model, the term $1 - 3\cos^2\Psi$ was assumed to rise linearly with increasing pressure until a value of $\Psi = 90^\circ - \Theta$ is reached. This stage ends at a hydrostatic pressure of $\sigma_p = 8$ GPa (region **3** in figure 6). This process is irreversible: for pressures above 8 GPa, the uniaxial stress component t remains constant in value and direction (region **4** in figure 6).

Finally, the effects observed are not in contradiction to the thermodynamical law which says that the compressibility

$$\kappa = -\frac{1}{V}\left(\frac{\delta V}{\delta p}\right)_T$$

is always positive [28]. Materials with Poisson's ratios close to 0.5 are easily compressed in the direction of the applied stress (low Young's modulus), but show a strong expansion of lattice spacings perpendicular to the stress direction. All in all, the volume of such materials decreases with pressure. In the diffraction geometry used here, only lattice planes whose normals lie nearly perpendicularly to the stress direction can be detected.

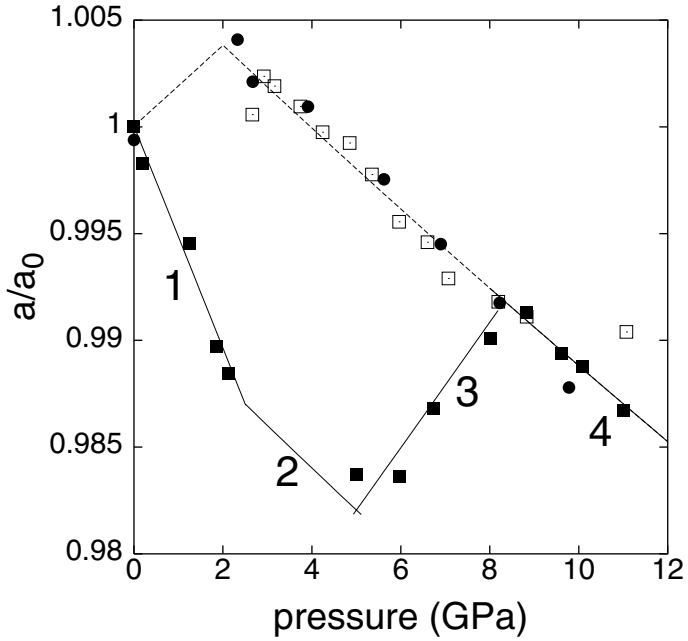

Figure 6. The hysteresis loop of Ti–Zr–Ni. The symbols are explained in the caption of figure 3. The numbers are explained in the text. The solid line is calculated using the model for pressure increase; the dotted line is calculated using the model described in the text during the pressure release and second pressure increase.

Acknowledgments

The authors would like to thank M Winzenick for help provided at the experimental station. We also acknowledge financial support from the German Academic Exchange Office (DAAD) and HASYLAB/DESY (Hamburg). Part of this work was supported by the BMBF project No 05ST8HRA 0.

Appendix

Poisson's ratio is defined as

$$\nu = -\frac{S_{12}}{S_{11}}. \tag{A.1}$$

The bulk modulus is

$$B_0 = \frac{1}{3(S_{11} + 2S_{12})}. \tag{A.2}$$

The shear modulus in elastically isotropic solids is

$$\mu = \frac{1}{2(S_{11} - S_{12})} \tag{A.3}$$

with S_{ij} being the elastic compliances.

References

[1] Shechtman D, Blech I, Gratias D and Cahn J W 1984 *Phys. Rev. Lett.* **53** 1951
[2] Sato-Sorensen Y and Sorensen L B 1989 *Phys. Rev.* B **39** 2654
[3] Johnson E, Staun Olsen J, Wood J V and Gerward L 1988 *Mater. Sci. Eng.* **99** 403
[4] Akahama Y, Mori Y, Kobayashi M, Kawamura H, Kimura K and Takeuchi S 1989 *J. Phys. Soc. Japan* **58** 2231
[5] Sadoc A, Itié J P, Polian A, Lefebvre S, Bessiere M and Calvayrac Y 1994 *Phil. Mag.* A **70** 855
[6] Lefebvre S, Bessiere M, Calvayrac Y, Itié J P, Polian A and Sadoc A 1995 *Phil. Mag.* A **72** 101
[7] Sadoc A, Itié J P, Polian A, Berger C and Poon S J 1998 *Phil. Mag.* A **77** 115
[8] Amazit Y, Perrin B, Fischer M, Itié J P and Polian A 1997 *Phil. Mag.* A **75** 1677
[9] Hasegawa M, Tsai A P, Kondo T, Yagi T and Kikegawa T 1999 *J. Non-Cryst. Solids* **250–252** 849
[10] Hasegawa M, Tsai A P and Yagi T 1999 *Phil. Mag. Lett.* **79** 691
[11] Kelton K F, Kim W J and Stroud R M 1997 *Appl. Phys. Lett.* **70** 3230
[12] Kelton K F and Gibbons P C 1997 *MRS Bull.* **22** 69
[13] Ponkratz U, Nicula R, Jianu A and Burkel E 1999 *J. Non-Cryst. Solids* **250–252** 844
[14] Nicula R, Jianu A, Ponkratz U and Burkel E 2000 *Phys. Rev.* B at press
[15] Otto J W, Vassiliou J K and Frommeyer G 1997 *J. Synchrotron Radiat.* **4** 152
[16] Otto J W 1997 *Nucl. Instrum. Methods* A **384** 552
[17] Decker D L 1971 *J. Appl. Phys.* **42** 3239
[18] Mao H K, Bell P M, Shaner J W and Steinberg D J 1978 *J. Appl. Phys.* **49** 3276
[19] Cahn J W, Shechtman D and Gratias D 1986 *J. Mater. Res.* **1** 13
[20] Young D A 1991 *Phase Diagrams of the Elements* (Berkeley, CA: University of California Press)
[21] Singh A K and Kennedy G C 1974 *J. Appl. Phys.* **45** 4686
[22] Singh A K 1993 *J. Appl. Phys.* **73** 4278
[23] Quilichini M and Jansen T 1997 *Rev. Mod. Phys.* **69** 277
[24] Singh A K and Balasingh C 1994 *J. Appl. Phys.* **75** 4956
[25] Funamori N, Yagi T and Uchida T 1994 *J. Appl. Phys.* **75** 4327
[26] Demeshev G B, Sidrow V A, Tsiok O B, Goncharova V A and Dmitriev D R 1995 *Europhys. Lett.* **29** 19
This paper reports the density ρ, the bulk modulus B_0 and the sound velocities for longitudinal and transverse modes v_l and v_t for Al–Li–Cu. From these values, the shear modulus μ was calculated according to $(C_{11} - C_{12})/2 = \mu = \rho v_t^2$; Poisson's ratio ν was calculated using $\nu = C_{12}/(C_{11} + C_{12})$ with $C_{11} = \rho v_l^2$.
[27] Gschneidner K A 1964 *Solid State Physics* vol 16, ed F Seitz and D Turnbull (New York: Academic)
[28] Reif F 1985 *Fundamentals of Statistical and Thermal Physics* (Singapore: McGraw-Hill)